Zeolites

Deutsche Ausgabe: DOI: 10.1002/ange.201510726
Internationale Ausgabe: DOI: 10.1002/anie.201510726

Targeted Synthesis of Two Super-Complex Zeolites with Embedded Isoreticular Structures

Jiho Shin[+], Hongyi Xu[+], Seungwan Seo, Peng Guo, Jung Gi Min, Jung Cho, Paul A. Wright, Xiaodong Zou, and Suk Bong Hong**

Abstract: *A novel structural coding approach combining structure solution, prediction, and the targeted synthesis of new zeolites with expanding complexity and embedded isoreticular structures was recently proposed. Using this approach, the structures of two new zeolites in the RHO family, PST-20 and PST-25, were predicted and synthesized. Herein, by extending this approach, the next two higher generation members of this family, PST-26 and PST-28, have been predicted and synthesized. These two zeolites have much larger unit cell volumes (422655 Å^3 and 614912 Å^3, respectively) than those of the lower generations. Their crystallization was confirmed by a combination of both powder X-ray and electron diffraction techniques. Aluminate and water concentrations in the synthetic mixture were found to be the two most critical factors influencing the structural expansion of embedded isoreticular zeolites under the synthetic conditions studied herein.*

Zeolites and molecular sieves continue to be widely used in a variety of commercial applications, including ion exchange, separation, and catalysis. The unique shape-selective properties of these microporous materials depend primarily on the size, shape, and/or dimensionality of their cavities and channels. As a result, much attention has been paid to the search for new types of zeolite structures over the last decades.[1–3] Although several millions of structures have been predicted upon developing more efficient computational and enumeration methods and algorithms,[4–6] the number of zeolite framework type codes approved by the Structure Commission of the International Zeolite Association remains at only 230 or so.[7] Most of the zeolite structures synthesized directly in the laboratory have resulted from a conventional trial-and-error approach. This is also the case for the framework types derived from the rational synthetic strategies developed thus far. For example, the geometric correlation between the organic structure-directing agents (SDAs) encapsulated in the pores and the pore architecture of the resulting zeolite is generally loose, regardless of the size, shape, and rigidity of the organic SDAs employed.[1–3] Although the introduction of heteroatoms such as Ge into silicate frameworks can direct the formation of particular zeolite building units, such as double 4 rings[8] and double 3 rings,[9] it is far from targeted synthesis of zeolites with specifically designed structures.

Very recently, we have reported the crystal structure of zeolite ZSM-25 (framework type MWF),[10] a structure which remained unsolved for more than 30 years. Our structure determination included the combined use of single-crystal three-dimensional electron diffraction data and phase information derived from the known structure of paulingite (PAU) which was found to have identical structural coding to ZSM-25. A similarity in the structures of zeolite Rho (RHO), paulingite, and ZSM-25 allowed us to discover a new principle of structure expansion (Figure 1) and thus to define them as the RHO family of zeolites with embedded isoreticular structures. The structural expansion principle in the RHO family is substantially different from that normally found in metal–organic frameworks[11,12] in that the space between the scaffolds is filled by four other cage types to form a fully tetrahedrally coordinated framework, giving each of its members different framework topologies but the same maximum ring size.

We were also able to predict the structures of two higher generations of the RHO family of zeolites with increased complexity, denoted RHO-G5 and RHO-G6.[10] These structures were then synthesized through a rational approach, with the synthesized structures denoted PST-20 and PST-25, respectively. The structure prediction was based on the strong reflections approach, that is, similar distribution of diffraction intensities in reciprocal space of the zeolites in the RHO family. In this Communication we report the prediction of the next two even more complex generations (RHO-G7 and RHO-G8; see Figure S1 in the Supporting Information) of the RHO family based on a new and simpler approach in comparison to the strong reflections approach used previously.[10] We also show that the structures can be synthesized by varying the concentrations of inorganic components in the

[*] Dr. J. Shin,[+] S. Seo, J. G. Min, J. Cho, Prof. S. B. Hong
Center for Ordered Nanoporous Materials Synthesis
School of Environmental Science and Engineering, POSTECH
Pohang 790-784 (Korea)
E-mail: sbhong@postech.ac.kr
Dr. H. Xu,[+] P. Guo, Prof. X. Zou
Inorganic and Structural Chemistry and Berzelii Center EXSELENT on Porous Materials, Department of Materials and Environmental Chemistry, Stockholm University
10691 Stockholm (Sweden)
E-mail: xzou@mmk.su.se
Prof. P. A. Wright
EaStCHEM School of Chemistry, University of St. Andrews
St. Andrews, Fife KY16 9ST (UK)
Dr. J. Shin[+]
Present address: Inorganic and Structural Chemistry and Berzelii Center EXSELENT on Porous Materials, Department of Materials and Environmental Chemistry, Stockholm University
10691 Stockholm (Sweden)
[+] These authors contributed equally to this work.

Supporting information for this article can be found under: http://dx.doi.org/10.1002/anie.201510726.

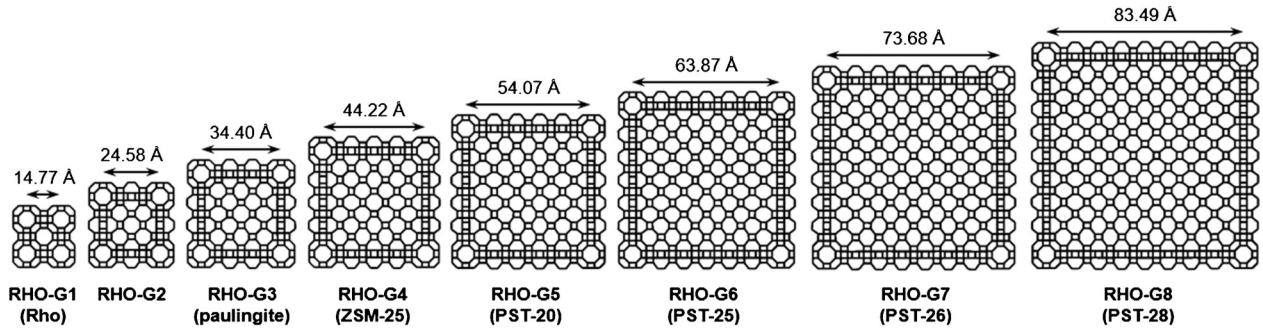

Figure 1. Framework representations of cross-sections (circa 12 Å thick) of RHO-G1 to RHO-G8 in the RHO family of zeolites. Structures RHO-G7 and RHO-G8 were predicted and then synthesized in this work.

synthetic mixture yielding PST-20. The formation of these targeted materials has been confirmed not only by LeBail refinement of the synchrotron powder X-ray diffraction (XRD) patterns of crystallized products, but also by selected area electron diffraction (SAED) patterns, from which the structural information on the scaffold expansion along each unit-cell edge and the manner of inter-scaffold space filling in the RHO family of zeolites can be directly obtained.

The scaffold of the RHO family, which constitutes $[4^{12}6^8 8^6]$ (*lta*), $[4^8 8^2]$ (*d8r*), and $[4^{12}8^6]$ (*pau*) cages, can be expanded by continuously adding an extra pair of *pau* and *d8r* cages along each unit-cell edge, as noted in our recent work.[10] Although the strong reflections approach in reciprocal space can be applied to predict higher generations of the RHO family, the procedures get more complex with the increasing number of symmetry independent atoms to be located in the electron density maps.

Herein we have developed a new and more convenient model building approach based on the structural coding in real space. Since both sets of scaffold and embedded cages in this family are repetitive, the appropriate structure fragments of RHO-G7 and RHO-G8 were predicted from their lower generations, that is, RHO-G6 (PST-25) and RHO-G7, respectively. The detailed prediction procedures can be found in the Supporting Information. The asymmetric units of RHO-G7 and RHO-G8 have 72 and 104 topologically distinct tetrahedral atoms, together with 168 and 240 such O atoms (Tables S1–S3). When inspecting the evolution of cage types within members of the RHO family, we found that the numbers of three embedded cages, that is, $[4^6 8^4]$ (*t-gsm*), $[4^5 8^3]$ (*t-oto*), and $[4^7 8^5]$ (*t-phi*) cages, increase much more rapidly than those of the other cage types (*lta*, *d8r*, *pau*, and $[4^6 6^2 8^6]$ (*t-plg*)) as the members become more complex. For example, ZSM-25 consists of 60 *t-gsm*, 144 *t-oto*, and 72 *t-phi* cages per unit cell, whereas RHO-G5 and RHO-G6 consist of 168 and 360 *t-gsm*, 240 and 360 *t-oto*, and 144 and 240 *t-phi* cages per unit cell, respectively. Furthermore, RHO-G7 and RHO-G8 constitute 660 and 1092 *t-gsm*, 504 and 672 *t-oto*, and 360 and 504 *t-phi* cages per unit cell, respectively (Table S4). Additionally, the unit cell volumes of RHO-G7 and RHO-G8 were calculated as 422655 $Å^3$ and 614912 $Å^3$, which are, respectively, about 1.5 and 2.2 times larger than the volume of PST-25 (275132 $Å^3$), the largest zeolite structure known to date. The simulated powder XRD patterns of RHO-G7 and RHO-G8 are given in Figure S2.

Previously, the rapid increase of the numbers of *t-gsm*, *t-oto*, and *t-phi* cages with the higher generations of the RHO family inspired us to search for zeolites that contain those cages. We found that natural zeolites gismondine (GIS) contains only *t-gsm* cages, whereas the phillipsite (PHI) contains *t-oto* and *t-phi* cages as building units. GIS and PHI zeolites are reported to possess substantial amounts of Ca^{2+} and even Ba^{2+} ions as extra framework cations.[13,14] To promote the crystallization of higher generations of the RHO family, therefore, we introduced a small amount of alkaline earth cations, especially Ca^{2+} and Sr^{2+}, into the ZSM-25 synthesis mixture. This rational approach finally allowed us to synthesize the two more complex zeolites, PST-20 (RHO-G5) and PST-25 (RHO-G6), respectively.[10]

The TEA^+-mediated syntheses (TEA^+ = tetraethylammonium) of the RHO family of zeolites (that is, ECR-18 (RHO-G3), ZSM-25 (RHO-G4), PST-20 (RHO-G5), and PST-25 (RHO-G6)) reported thus far reveal that the phase selectivity of the crystallization differs notably according to the SiO_2/Al_2O_3 and H_2O/SiO_2 ratios in the synthetic mixture, as well as with the type of inorganic cations employed.[10,15–17] Thus, our initial attempts to synthesize the predicted RHO-G7 and RHO-G8 structures involved variation of the water and aluminate contents in the synthetic mixture. Table 1 lists the representative products from syntheses in the mixed TEA^+-Na^+-Ca^{2+} SDA system and aluminosilicate gels in which the SiO_2/Al_2O_3 and H_2O/SiO_2 ratios are in the ranges 4.8–14.4 and 20.8–54.2, respectively. The phase selectivity of the crystallization is very sensitive to both SiO_2/Al_2O_3 and H_2O/SiO_2 ratios in the gel. When the initial SiO_2/Al_2O_3 ratio in the gel was fixed to 7.2, for example, a decrease in H_2O/SiO_2 ratio resulted in the formation of increasingly more complex generations of the RHO family. However, unlike ZSM-25 and PST-20,[10,16] the lower generations of this family of embedded isoreticular zeolites, we could only obtain them as their mixtures, together with a small amount of gismondine (Table 1). A plausible explanation for this will be given below.

When using an aluminosilicate gel with $H_2O/SiO_2 = 34.7$ (Table 1, run 3), we were able to find signs of the crystallization of RHO-G7, denoted PST-26. This suggests that a decrease in H_2O/SiO_2 ratio leads to the preferential

Table 1: Syntheses from gel composition 5.2 R·1.9 Na_2O·0.5 $Ca(NO_3)_2$·*x* Al_2O_3·7.2 SiO_2·*y* H_2O.[a]

Run	Gel composition SiO_2/Al_2O_3	H_2O/SiO_2	Product[b]
1	7.2	54.2	PST-20 + ZSM-25 + gismondine
2	7.2	41.7	PST-25 + PST-20 + gismondine
3	7.2	34.7	PST-26 + PST-25 + gismondine
4	7.2	27.8	gismondine + (PST-26) + (PST-25)
5	4.8	34.7	gismondine
6	4.8	27.8	gismondine
7	9.6	34.7	PST-25 + PST-26 + PST-20
8	9.6	27.8	PST-26 + PST-28 + PST-25
9	9.6	20.8	PST-26 + PST-28 + PST-25 + mordenite
10	14.4	34.7	mordenite + PST-25 + PST-20
11	14.4	27.8	mordenite + (PST-26) + (PST-25)

[a] R is tetraethylammonium bromide, and *x* and *y* are varied between $0.5 \le x \le 1.5$ and $150 \le y \le 390$, respectively. The final synthetic mixture was stirred at 80 °C for 24 h, and crystallization was performed under rotation (60 rpm) at 145 °C for 2 days. [b] The first phase listed was the major phase obtained, with products obtained in trace amounts given in parentheses.

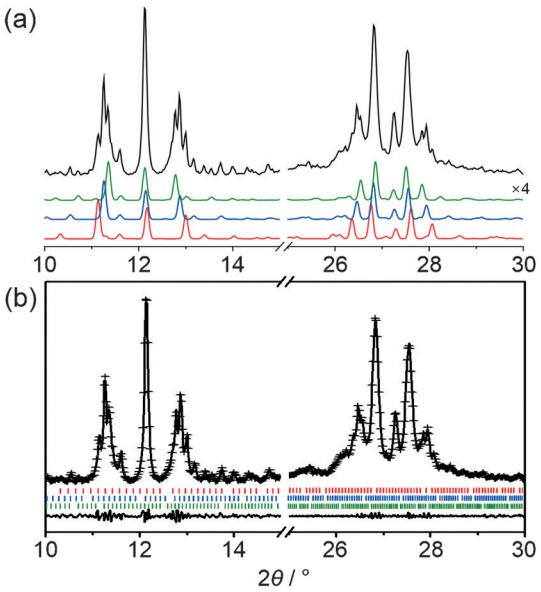

Figure 2. a) Synchrotron powder XRD patterns of the solid product obtained from run 8 in Table 1. The top trace shows the experimental data, whereas the bottom three traces show the simulated patterns for RHO-G6 (red), RHO-G7 (blue), and RHO-G8 (green), respectively ($\lambda = 1.4865$ Å). The intensity of the simulated PXRD patterns in the 25–30° region was enhanced 4-fold. b) Three-phase (PST-25, PST-26, and PST-28) LeBail fit for the same product, showing the experimental data (crosses), calculated fit (solid line), and difference plot (lower trace). Red, blue, and green vertical bars indicate the positions of Bragg peaks of PST-25, PST-26, and PST-28, respectively.

formation of *t-oto*, *t-gsm*, and *t-phi* cages over that of the other four types of cages (namely *lta*, *d8r*, *pau*, and *t-plg* cages), thus favoring the formation of more complex higher generations. However, a further decrease in H_2O/SiO_2 ratio to 27.8 in the gel yielded gismondine together with trace amounts of PST-25 and PST-26. Therefore, we carried out syntheses using aluminosilicate gels of varying SiO_2/Al_2O_3 ratios while keeping their H_2O/SiO_2 ratio to 34.7 or lower. Gismondine crystallized from synthetic mixtures with $SiO_2/Al_2O_3 = 4.8$ and $H_2O/SiO_2 \le 34.7$. As shown in Table 1, a reaction using a gel with $SiO_2/Al_2O_3 = 9.6$ and $H_2O/SiO_2 = 27.8$ gave a product containing RHO-G8 (PST-28), the next super-complex generation of the RHO family (Table 1, run 8). When the H_2O/SiO_2 ratio in the synthetic mixture was decreased further to 20.8 under the conditions mentioned above, mordenite (MOR) began to appear. A further increase in the SiO_2/Al_2O_3 ratio to 14.4 yielded a mixture of mordenite and the RHO family of zeolites.

Figure 2 shows the selected regions ($2\theta = 10$–$15°$ and 25–30°) of the synchrotron powder XRD pattern of the product obtained from run 8 in Table 1. Included for comparison are the simulated XRD patterns of hypothetical zeolite structures RHO-G6, RHO-G7, and RHO-G8. It can be seen that this product is a mixture of RHO-G6 (PST-25, circa 20%), RHO-G7 (PST-26, circa 45%), and RHO-G8 (PST-28, circa 35%; Figure S3). As shown in Figure 2 and in Figure S4, the three-phase LeBail refinement based on PST-25, PST-26, and PST-28 shows good agreement between the experimental and calculated profiles ($R_{wp} = 0.0190$, $R_p = 0.0131$). The lattice parameters obtained were $a = 65.03969(6)$ Å for PST-25, $a = 75.0462(5)$ Å for PST-26, and $a = 85.0363(5)$ Å for PST-28.

It is also remarkable that the Na^+-exchanged form of the product from run 8 is characterized by a CO_2 uptake of 2.6 mmol g^{-1} at 1.0 bar and 25 °C, which is somewhat lower than the uptakes (≤ 3.2 mmol g^{-1}) of the lower, pure generations of the RHO family of zeolites, such as ZSM-25 and Na-PST-20 (Figure S5).[10] As this product, as well as the product obtained from run 7 (containing a physical mixture of PST-25, PST-26, and PST-20), loses crystallinity after calcination under flowing air at 550 °C for 6 h (as occurs with PST-20), the higher generations of this family may, in our view, have poorer structural stability than the lower generations. If such is the case, this would then rationalize the relatively low CO_2 uptake of the product obtained from run 8.

Figure 3 shows the SAED patterns of PST-26 and PST-28 crystals of the product obtained from run 8, recorded along both the [111] and [001] zone axes. As recently reported,[10] the intensity distributions of reflections observed in the SAED patterns of these materials are similar to each other because of the strong similarities between the manner of scaffold expansion and how the inter-scaffold space is filled. The SAED patterns of PST-26 are characterized by the structure relation $d_{(10\text{-}1)} = d_{(\text{-}110)} = d_{(110)} = 52.71(5)$ Å, implying that $a = 74.53(9)$ Å. Similarly, those of PST-28 show that $d_{(10\text{-}1)} = d_{(\text{-}110)} = d_{(110)} = 60.60(6)$ Å and thus $a = 85.69(7)$ Å. The fact these lattice parameters are in excellent agreement with the powder XRD results confirms the successful crystallization of both of the predicted phases RHO-G7 (PST-26) and RHO-G8 (PST-28).

Another important experimental result that can be extracted from Figure 3 is that the number of weak reflections between the strong reflections differs systematically according to the generation number of the given member of the RHO family. In the SAED patterns of ZSM-25 and PST-20 taken along the [111] zone axis, for example, there are two/three and three/four weak reflections between two strong

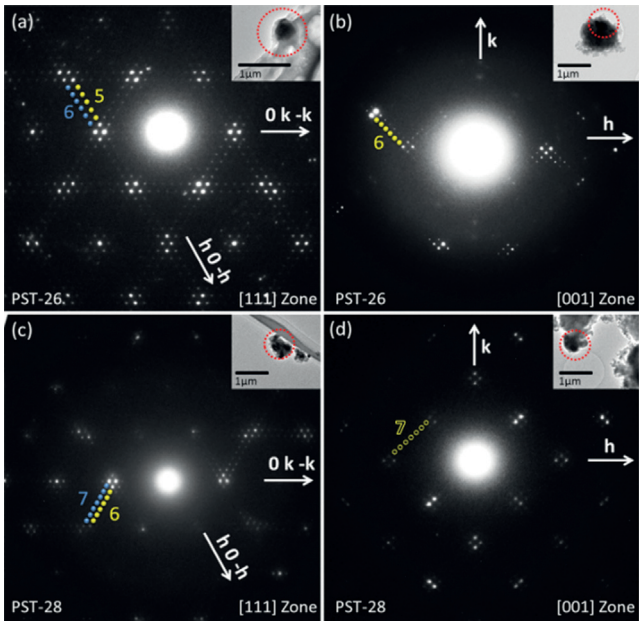

Figure 3. SAED patterns of PST-26 (a, b) and PST-28 (c, d) along the [111] (a, c) and [001] (b, d) zone axes, respectively. The number of weak diffraction spots is marked to show the distinguishable structural features of both zeolites. Since the weak diffraction spots in (d) are not observable, the distance between two closest strong diffraction spots is used to predict the expected position of weak spots.

reflections, respectively (Figure S6). Moreover, four/five, five/six, and six/seven weak reflections are observable between each pair of strong reflections in the patterns of PST-25, PST-26, and PST-28, respectively. This trend of the increasing number of weak reflections between the strong reflections also holds for the SAED patterns taken along the *c* axis.

Despite the considerable synthetic efforts, none of our attempts to crystallize PST-25, PST-26, and PST-28 in their pure forms have yet been successful, in contrast to the cases of ZSM-25 and PST-20.[10,16] We think that this may be attributed to the similarity in the thermodynamic stabilities of compounds. As shown in Figure 4, in fact, the energy difference between two adjacent generations, calculated using the program GULP,[18] becomes gradually smaller as the generation number (n) of the members (RHO-Gn) of the RHO family of zeolites increases. Therefore, it appears to become more difficult to obtain the pure form of higher generation members with increasing the generation number at least in the mixed TEA^+-Na^+-Ca^{2+} (or the other alkaline earth cations) SDA system. In our view, a similar trend may also be observed for other families of zeolites with embedded isoreticular structures, especially when their members are synthesized in similar SDA systems.

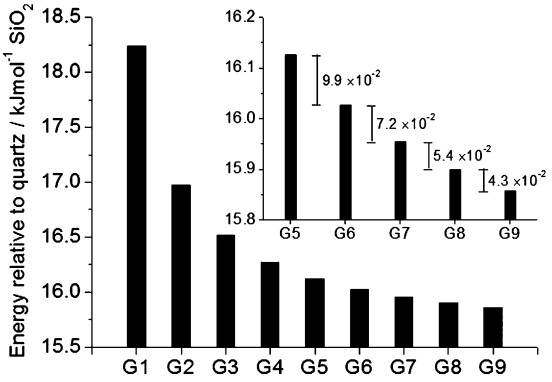

Figure 4. Lattice energies relative to quartz of the RHO-Gn structures in the RHO family calculated by GULP.[18] Inset: an expanded portion of the histogram showing more clearly the relative energies of the higher generation structures.

In summary, we have predicted and subsequently successfully synthesized two more complex, higher generations of the RHO family of zeolites, denoted PST-26 and PST-28, respectively. The overall results of this work, as well as those of our recent study,[10] demonstrate that the type and concentration of inorganic cations and the aluminate and water concentrations in the synthetic mixtures (containing TEA^+ ions as an organic SDA) are critical factors affecting the structural complexity of crystallized embedded isoreticular zeolites. We anticipate that our structural coding concept will further be used to achieve the "fully rational" synthesis of zeolites with designed structures and properties.

Acknowledgements

This work was supported by the NCRI (2012R1A3A-2048833) and BK 21-plus programs through the National Research Foundation of Korea, the Swedish Research Council (VR), the Swedish Governmental Agency for Innovation Systems (VINNOVA), the Röntgen-Ångström Cluster through project grant MATsynCELL, and the Knut and Alice Wallenberg Foundation through project grant 3DEM-NATUR. We thank PAL (Pohang, Korea) for synchrotron diffraction beam time. PAL is supported by MSIP and POSTECH.

Keywords: microporous materials · structure prediction · synthesis design · X-ray diffraction · zeolites

How to cite: *Angew. Chem. Int. Ed.* **2016**, *55*, 4928–4932
Angew. Chem. **2016**, *128*, 5012–5016

[1] M. A. Camblor, S. B. Hong in *Porous Materials* (Eds.: D. W. Bruce, D. O'Hare, R. I. Walton), Wiley, Chichester, **2011**, pp. 265–325.
[2] M. Moliner, F. Rey, A. Corma, *Angew. Chem. Int. Ed.* **2013**, *52*, 13880–13889; *Angew. Chem.* **2013**, *125*, 14124–14134.
[3] M. Moliner, C. Martinez, A. Corma, *Angew. Chem. Int. Ed.* **2015**, *54*, 3560–3579; *Angew. Chem.* **2015**, *127*, 3630–3649.
[4] M. M. J. Treacy, I. Rivin, E. Balkovsky, K. H. Randall, M. D. Foster, *Microporous Mesoporous Mater.* **2004**, *74*, 121–132.
[5] R. Pophale, P. A. Cheeseman, M. W. Deem, *Phys. Chem. Chem. Phys.* **2011**, *13*, 12407–12412.
[6] a) J. V. Smith, *Chem. Rev.* **1988**, *88*, 149–182; b) M. O'Keeffe, S. T. Z. Hyde, *Z. Kristallogr.* **1996**, *211*, 73–78; c) O. D. Friedrichs, A. W. M. Dress, D. H. Huson, J. Klinowski, A. L. Mackay, *Nature* **1999**, *400*, 644–647; d) M. D. Foster, M. M. J. Treacy, J. B. Higgins, I. Rivin, E. Balkovsky, K. H. Randall, *J. Appl. Crystallogr.* **2005**, *38*, 1028–1030.

[7] International Zeolite Association, Structure Commission, http://www.iza-structure.org.
[8] L. Tang, L. Shi, C. Bonneau, J. L. Sun, H. J. Yue, A. Ojuva, B. L. Lee, M. Kritikos, R. G. Bell, Z. Bacsik, J. Mink, X. D. Zou, *Nat. Mater.* **2008**, *7*, 381 – 385.
[9] Y. Yun, M. Hernández, W. Wan, X. Zou, J. L. Jordá, A. Cantín, F. Rey, A. Corma, *Chem. Commun.* **2015**, *51*, 7602 – 7605.
[10] P. Guo, J. Shin, A. G. Greenaway, J. G. Min, J. Su, H. J. Choi, L. Liu, P. A. Cox, S. B. Hong, P. A. Wright, X. Zou, *Nature* **2015**, *524*, 74 – 78.
[11] M. Eddaoudi, J. Kim, N. Rosi, D. Vodak, J. Wachter, M. O'Keeffe, O. M. Yaghi, *Science* **2002**, *295*, 469 – 472.
[12] H. Deng, S. Grunder, K. E. Cordova, C. Valente, H. Furukawa, M. Hmadeh, F. Gándara, A. C. Whalley, Z. Liu, S. Asahina, H. Kazumori, M. O'Keeffe, O. Terasaki, J. F. Stoddart, O. M. Yaghi, *Science* **2012**, *336*, 1018 – 1023.
[13] K. Fischer, V. Schramm, *Adv. Chem. Ser.* **1971**, *101*, 250 – 258.
[14] R. Rinaldi, J. J. Pluth, J. V. Smith, *Acta Crystallogr. Sect. B* **1974**, *30*, 2426 – 2433.
[15] D. E. W. Vaughan, K. G. Strohmaier, *Microporous Mesoporous Mater.* **1999**, *28*, 233 – 239.
[16] S. B. Hong, W. C. Paik, W. M. Lee, S. P. Kwon, C.-H. Shin, I.-S. Nam, B.-H. Ha, *Stud. Surf. Sci. Catal.* **2001**, *135*, 186 – 193.
[17] D. J. Kim, C.-H. Shin, S. B. Hong, *Microporous Mesoporous Mater.* **2005**, *83*, 319 – 325.
[18] J. D. Gale, A. L. Rhol, *Mol. Simul.* **2003**, *29*, 291 – 341.

Received: November 19, 2015
Published online: March 15, 2016

